Kinetics of the Reactions of the $CHBr_2$ and $CHBr_2O_2$ Radicals with O_2 and NO

Kyle D. Bayes,* Randall R. Friedl, and Stanley P. Sander

Jet Propulsion Laboratory, California Institute of Technology, Pasadena, California 91109

Received: November 10, 2004; In Final Form: February 2, 2005

When bromoform ($CHBr_3$) is photolyzed at 266 or 303 nm in the presence of O_2 and NO, the formation of secondary Br atoms is observed. By following the rate of growth of this secondary Br atom signal as a function of conditions, rate constants have been determined for the reactions $CHBr_2 + O_2$, $CHBr_2 + NO$ (both pressure-dependent), and $CHBr_2O_2 + NO$ ($k_{2a} = (1.74 \pm 0.16) \times 10^{-11}$ cm^3 molecule^{-1} s^{-1} at 23 °C). By measuring the amplitude of the secondary Br signal compared to the primary Br formed in the initial photolysis, it is established that the $CHBr_2O$ radical spontaneously decomposes to form $CHBrO + Br$ at least 90%, and probably 100%, of the time, in agreement with previous work and with recent ab initio calculations. A survey of four other polybrominated methanes, CH_2Br_2, $CHClBr_2$, CF_2Br_2, and CBr_4, shows that they all generate secondary Br atoms when photolyzed at 266 nm in the presence of O_2 and NO, suggesting that their reaction sequences are similar to that of bromoform.

Introduction

The bromoform ($CHBr_3$) observed in the earth's atmosphere originates mostly from algae and plankton in the oceans.[1−3] Although the observed concentrations are very small, in the parts per trillion range, bromoform has been of interest recently because bromine is a very potent catalyst for the destruction of ozone.[4−6]

In the troposphere bromoform is destroyed by reaction with OH radicals (∼25%) and by photolysis at wavelengths ≥ 300 nm (∼75%).[4] Our previous work measured the quantum yields for bromine atom formation when bromoform is photolyzed in the ultraviolet.[7] For wavelengths longer than 300 nm, the quantum yield for Br formation, Φ(Br), is unity or close to unity. At 266 nm, however, Φ(Br) is only 0.76, suggesting a second channel such as $HBr + CBr_2$ or $Br_2 + CHBr$. A recent beam study at 267 nm observed a signal from Br_2 corresponding to the latter channel.[8]

In the upper troposphere and lower stratosphere, photolysis at wavelengths longer than 300 nm is the dominant loss mechanism for bromoform.[4] In air, one expects that the resulting $CHBr_2$ radicals will be rapidly converted to peroxy radicals, $CHBr_2O_2$. The present manuscript describes some reactions of the $CHBr_2$ and $CHBr_2O_2$ radicals and shows how these can generate additional Br atoms.

Description of Experiments

The apparatus used for these experiments has been described previously.[7] Briefly, the gas mixture flowed through an aluminum tube, 5 cm × 5 cm × 26 cm, with the laser beam traversing the long axis. A discharge source of atomic bromine resonance radiation (near 130 and 160 nm) oriented perpendicular to the laser beam illuminated the center of the flow tube. A solar blind photomultiplier tube (PMT) viewed the region of overlap between laser beam and lamp radiation. Bromine atoms formed in the flow tube scattered the resonance radiation, and some of the scattered photons entered the PMT. Output pulses from the PMT were counted as a function of time and stored on a computer. Results from 1000 to 6000 laser pulses were added before analysis.

Only differences from our previous study[7] will be described below. The new bromine resonance lamp used a flowing mixture of Br_2 in He. This mixture was made continuously by flowing 3.8 cm^3 s^{-1} of He at 730 Torr past a diffusion source of Br_2, which consisted of a reservoir of liquid Br_2 at 23 °C connected to the He flow by a capillary 0.3 mm in diameter and 5 cm in length. Most of the resulting mixture, containing about 5 ppm Br_2, was discarded into the hood, but a small amount flowed into the lamp, which operated at a pressure of 2.5 Torr. The maximum possible [Br] in the discharge was about 10^{12} cm^{-3}. As before, the discharge was maintained by 10 W of RF power at 180 MHz, and the window was MgF_2.

A new solar blind PMT (Electron Tubes 9403B) having a CsI photocathode and MgF_2 window was used to detect the Br resonance fluorescence. The output pulses went to an amplifier−discriminator (Ortec 9302) before being counted as a function of time (Ortec MCS-pci).

Two wavelengths were used for photolyzing the bromoform, 266 and 303 nm. The 266 nm pulses from the YAG laser passed through a ×3 beam expander to give a beam with a diameter of 1.5 cm. The pulses were limited in energy so that, for the bromoform concentrations used, the initial $CHBr_2$ radical concentrations were ≤10^{11} cm^{-3} (<0.3 mJ at 10 Torr to <1 mJ at 2 Torr). The 303 nm pulses were generated by doubling the output of a YAG-pumped dye laser (PDL 3, sulforhodamine 640 dye). The ×3 beam expander was also used on the 303 nm pulses, but the expanded beam was only about 0.6 cm in diameter. Since the bromoform cross-section at 303 nm is 100 times smaller than that at 266 nm,[9] the maximum pulse energies at 303 nm, 1.5−1.8 mJ, were used. Even with the more intense pulses and longer integration times, the signal-to-noise ratio at 303 nm was about a factor of 10 less than at 266 nm. Increasing the bromoform concentrations did not improve the signals significantly because of strong attenuation of the bromine resonance radiation by $CHBr_3$.

The gases, all from Air Products, were used without further purification: N_2 (UPC, 99.9993%); air (UPC, 99.9995%); O_2 (UPC, 99.996%); He (Research Grade, 99.9999%). The main

* To whom correspondence should be addressed. Fax: (818) 393-5019. E-mail: kdbayes@jpl.nasa.gov.

10.1021/jp044842m CCC: $30.25
Published on Web 03/10/2005

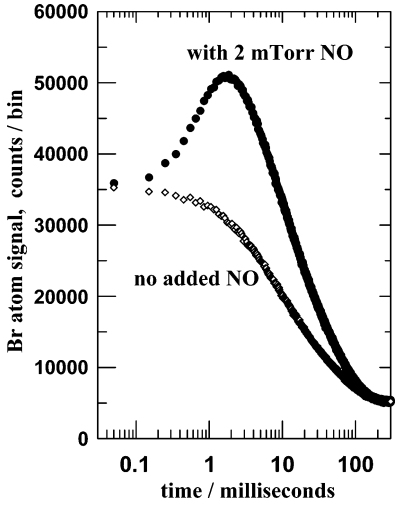

Figure 1. Resonance fluorescence signal from Br atoms as a function of time after the laser pulse. The conditions were as follows: $[CHBr_3] = 8 \times 10^{14}$ cm^{-3}; $[NO] = 6 \times 10^{13}$ cm^{-3} (solid circles only); balance air; total pressure, 4.05 Torr; 23 °C; laser energy, 0.6 mJ pulse^{-1} at 266 nm; 3 Hz. Dwell time was 100 μs bin^{-1}, and 2000 sweeps have been added. The initial [Br] was about 2×10^{11} cm^{-3}.

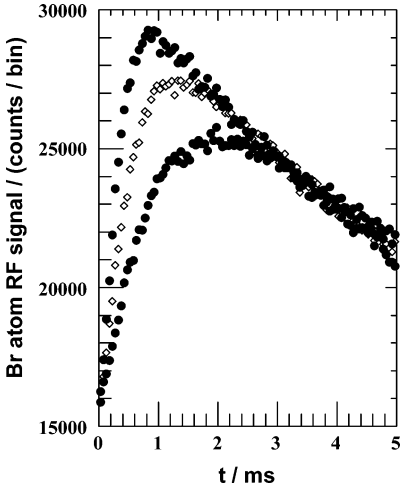

Figure 2. RF signal when photolyzing $CHBr_3$ at 266 nm and 2 Torr for different NO concentrations. From top to bottom: $[NO] = 3.12 \times 10^{14}$, 1.27×10^{14}, and 6.3×10^{13} molecules cm^3; balance, O_2. Background counts have been subtracted from each data set, and then they have been normalized to a common S_o. The initial [Br] was about 1×10^{11} cm^{-3}.

carrier gas (N_2, air, or O_2) was bubbled through bromoform (Aldrich, 99+%) at about 20 °C and 730 Torr. Some of this entered the flow system through a flow controller, while the excess went to a hood. Gas chromatographic analysis of the $N_2/CHBr_3$ mixture showed a trace of CH_2Br_2 (<0.4% of the $CHBr_3$) and no detectable CBr_4. Separate flow controllers were used to add O_2 and a NO/He mixture to the flow system. Pressures were monitored with recently calibrated gauges (MKS Baratron).

A commercial mixture of NO in He was used (Air Products, nominally 10.1% NO). To calibrate, 108 Torr of the mixture was added to an evacuated 5 L bulb and then pure O_2 was added to give a total pressure of 997 Torr. This secondary mixture was allowed to mix and react in the dark for 60 h. Samples of this secondary mixture were then transferred to a 10 cm cell, and the NO_2 absorption was measured with a spectrophotometer (Cary 4E) at a resolution of 0.2 nm. Using the NO_2 cross-sections recommended by Vandaele et al.[10] and making the necessary corrections for dimerization to N_2O_4, the original NO/He mixture was determined to be 10.97 mol % NO (standard deviation, 0.03%; $N = 13$).

Observation and Model

Preliminary experiments showed that when bromoform was photolyzed in N_2 or in air, the bromine atom signal appeared immediately after the laser pulse, as shown in the lower trace in Figure 1. The signal then decayed monotonically as the atoms diffused out of the observation zone and were lost to the walls. However, when small concentrations of NO were present together with significant concentrations of O_2, a secondary generation of bromine atoms was observed, as shown in the upper trace in Figure 1. Note that the two signals in Figure 1 have the same initial value, showing that the initial photolytic formation of Br atoms is the same, and also they decay to the same background level at long times.

The absolute concentrations of Br atoms were not determined in the present experiments. Only the relative Br concentrations were measured by using the resonance fluorescence (RF) signal. Early experiments established that the jump in the RF signal immediately after the laser pulse was proportional to the laser intensity (0.2−1.5 mJ/pulse) and also to the bromoform concentration. The rate of rise of the secondary bromine atom signal was faster the larger the NO concentration, as shown in Figure 2.

On the basis of these observations, the known reactivity of peroxy radicals with NO, and a previous study of the chemistry of the $CHBr_2$ radical,[11] the following mechanism was used to model the behavior of this system.

Initiation:

$$CHBr_3 + h\nu \rightarrow CHBr_2 + Br$$

Stage 1:

$$CHBr_2 + O_2 + M \rightarrow CHBr_2O_2 + M \quad (1a)$$

$$CHBr_2 + NO + M \rightarrow CHBr_2NO + M \quad (1b)$$

$$CHBr_2 \rightarrow \text{diffusional loss} \quad (1c)$$

Stage 2:

$$CHBr_2O_2 + NO \rightarrow CHBr_2O + NO_2 \quad (2a)$$

$$CHBr_2O_2 \rightarrow \text{diffusional loss} \quad (2b)$$

$$CHBr_2O \rightarrow CHBrO + Br \quad (2c)$$

Stage 3:

$$Br \rightarrow \text{diffusional loss} \quad (3)$$

The kinetics of this system can be grouped by losses of the $CHBr_2$ radical (stage 1), losses of the $CHBr_2O_2$ radical (stage 2), and loss of the bromine atoms (stage 3). Following the initiation of the reactions by the laser pulse, the dominant reaction of $CHBr_2$ radicals is the three-body combination with O_2 to form peroxy radicals (reaction 1a). Since NO is also present, and since methyl radicals are known to undergo a three-body reaction with NO,[12] reaction 1b is included as a competing loss process. Also, $CHBr_2$ may diffuse out of the observation region, reaction 1c.

Stage 2 involves loss processes for the $CHBr_2O_2$ radicals. Since our experiments are done in the 2−10 Torr range, we

only include the direct reaction of the peroxy radical with NO to form NO_2 and the dibromomethoxy radical, $CHBr_2O$ (reaction 2a). At much higher pressures stabilization to the peroxynitrite or nitrate would need to be included. The $CHBr_2O_2$ radicals can also be lost by diffusion, reaction 2b.

The source of the secondary Br atoms observed in Figures 1 and 2 is assumed to be reaction 2c. Orlando et al.[11] concluded, on the basis of analysis of stable products, that any dibromomethoxy radicals ($CHBr_2O$) formed in their system were decomposing to CHBrO + Br, even at 700 Torr. For our much lower pressures, we assume that decomposition is the exclusive fate of $CHBr_2O$ radicals. This critical assumption will be tested when analyzing the data.

Stage 3 involves just the diffusional loss of Br atoms from the detection region. No radical−radical reactions, such as $CHBr_2 + CHBr_2$ or $Br + CHBr_2O_2$, have been included in the above reaction scheme. For the present experiments, the maximum initial radical concentrations were $\leq 10^{11}$ cm^{-3} for the 266 nm experiments and were a factor of 3−10 lower for 303 nm experiments. Even if the radical−radical reactions occur on every collision, their rates should be negligible compared to those of other radical-loss reactions given above.

The differential equations corresponding to the above mechanism can be integrated analytically to give (subscripts on rate constants refer to reaction numbering in the model):

$$[\mathrm{Br}] = [\mathrm{Br}]_o \exp(-k_3 t) + \{([\mathrm{Br}]_o F_1 F_2)(K_1 K_2)/(K_1 - K_2)\}\{M_{13}/(K_1 - k_3) - M_{23}/(K_2 - k_3)\} \quad \text{(I)}$$

where

$$K_1 = k_{1a}[\mathrm{O_2}] + k_{1b}[\mathrm{NO}] + k_{1c}$$

$$K_2 = k_{2a}[\mathrm{NO}] + k_{2b}$$

$F_1 = k_{1a}[\mathrm{O_2}]/K_1 =$ fraction of $CHBr_2$ that forms $CHBr_2O_2$

$F_2 = k_{2a}[\mathrm{NO}]/K_2 =$ fraction of $CHBr_2O_2$ that forms $CHBr_2O$

$$M_{13} = \{\exp(-k_3 t) - \exp(-K_1 t)\}$$

$$M_{23} = \{\exp(-k_3 t) - \exp(-K_2 t)\}$$

$[\mathrm{Br}]_o = [\mathrm{CHBr_2}]_o =$ initial concentrations formed by laser pulse

To fit the experimental data, several modifications were made to eq I. Since only the RF signal, *S*, is being measured, and not the absolute concentrations, *S* is used in place of [Br] in eq I. Similarly, S_0 is substituted for the initial concentration, $[\mathrm{Br}]_o$. Also a constant term, *Bk*, was added to account for the background signal, which was caused by scattered light from the lamp entering the PMT detector.

A single fitted constant, S_1, was substituted for the product $([\mathrm{Br}]_o F_1 F_2)$; in this way the requirement that every $CHBr_2O$ radical decomposes to give one additional Br atom is relaxed. Then in the data analysis the fitted values for S_1 will be compared to the fitted and calculated values of the product $(S_0 F_1 F_2)$ in order to test the assumption that every $CHBr_2O$ radical decomposes rapidly.

The decay of the RF signal at long times did not follow a single exponential as given in eq I. The observed decays were more complex, requiring three different exponentials having rate constants $k_{3a} > k_{3b} > k_{3c}$ with amplitudes F_a, F_b, and F_c. F_a was taken to be unity, and F_b and F_c were fitted for each data set.

As a result of these changes, the working equation used for fitting the experimental data was

$$S = S_0 M_{abc} + S_1\{K_1 K_2/(K_1 - K_2)\}\{M_1/(K_1 - k_{3a}) - M_2/(K_2 - k_{3a})\} + Bk \quad \text{(II)}$$

where, now,

$$M_{abc} = \exp(-k_{3a} t) + F_b M_{ba} + F_c M_{cb}$$

$$M_{ba} = \exp(-k_{3b} t) - \exp(-k_{3a} t)$$

$$M_{cb} = \exp(-k_{3c} t) - \exp(-k_{3b} t)$$

$$M_1 = M_{abc} - \exp(-K_1 t)$$

$$M_2 = M_{abc} - \exp(-K_2 t)$$

Although not evident at first glance, eq II is symmetric in K_1 and K_2, the two constants that control the rise time of the secondary Br generation. This means that if eq II is successfully fit to a data set, it is not possible to know from that one data set which value is K_1 and which is K_2. This ambiguity was handled in the following manner. Experiments were done so that either K_1 was significantly greater than K_2 or vice versa. For example, in the experiment shown in Figure 1, the 0.8 Torr of O_2 present with only a small concentration of NO results in $K_1 \gg K_2$. As a consequence of this disparity, the observed rise time is controlled mainly by K_2 (the "rate-determining step"). Doing a series of experiments with varying [NO], all with large $[O_2]$, allows the values of k_{2a} and k_{2b} to be determined. Similarly, experiments with large, but not too large, [NO] and small and varying $[O_2]$ can give values for k_{1a}, k_{1b}, and k_{1c}.

In using the above scheme to evaluate rate constants, a *numerical* value for either K_1 or K_2, whichever was larger, was inserted into eq II before doing the least-squares fit to a data set. This numerical value for K_1 or K_2 was calculated for each experiment using preliminary values of the rate constants (initially guesses). For example, with large $[O_2]$, K_2 was determined as a function of [NO], giving preliminary values for k_{2a} and k_{2b}. These preliminary values were then used to calculate numerical values for K_2 for a different set of experiments in which $K_2 \gg K_1$, yielding a preliminary set of k_{1a}, k_{1b}, and k_{1c}. Then returning to the first set of experiments with $K_1 > K_2$, numerical values of K_1 were recalculated using the preliminary k_{1a}, k_{1b}, and k_{1c} and the least-squares calculations repeated to give improved values for K_2, and thus for k_{2a} and k_{2b}. This iteration was repeated until a self-consistent set of rate constants was established. Since the large value of K_1 or K_2 has only a minor effect on the observed rise time, usually only two or three iterations were necessary.

Using a numerical value for either K_1 or K_2 and fitting eq II to a data set resulted in nine fitted constants. Of these, S_0, S_1, K_1 or K_2, and *Bk* were the most important for determining rate constants and establishing the mechanism. The other five fitted constants, k_{3a}, k_{3b}, k_{3c}, F_b, and F_c were needed for the signal decay; these interacted only weakly with the first four parameters. For a series of experiments with similar concentrations, the five decay parameters were similar. Values of F_b were about 0.6−0.7 and for F_c were about 0.3. The two larger decay constants were pressure-dependent, as expected for diffusion-controlled processes; the product of pressure times k_{3a} was in

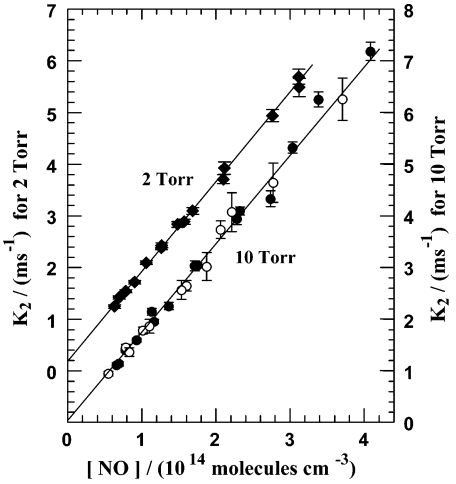

Figure 3. Dependence of K_2 on the NO concentration for experiments at 2 and 10 Torr. The open symbols are for photolysis at 303 nm, and the filled symbols are for 266 nm. The error bars represent one standard deviation as reported by the least-squares fitting program for each experiment. The solid lines are weighted linear least-squares fits.

the range of 700−900 Torr s^{-1}, while pressure times k_{3b} were 250−400 Torr s^{-1}. These two diffusion-controlled processes are needed to describe the loss of Br atoms out of the most sensitive region of detection, where the cone of radiation from the lamp intersects with the cone of view of the PMT. The fitted values of k_{3c} were not noticeably pressure-dependent but did seem to vary from day to day (6−30 s^{-1}). Probably this slow decay is following the loss of Br atoms on the walls of the flow tube.

Some data sets could be fit reasonably well with only two exponential decay terms instead of three. However, the data sets with the strongest signal-to-noise showed that the three exponential fits were superior (significantly lower χ^2) to the two exponential decay fits, so eq II was used for all of the data sets. Occasionally the least-squares fitting algorithm (PSI Plot, Version 7) would converge to a false minimum; this was evident both visually, when the resulting function was plotted, and numerically (reduced $\chi^2 > 1.2$), so that fit would be discarded and different starting parameters would be tried. Fits were accepted if the reduced χ^2 was between 0.9 and 1.2 and the difference plots showed no significant deviation from Poisson statistics.

Some of the runs at 303 nm with weak S_1 signals converged slowly or not at all; when this occurred, a numerical value for one or two of the decay parameters obtained from a run at 266 nm at the same pressure and with similar flow conditions was inserted into eq II. When this was done, the least-squares fits would converge rapidly and the resulting eight or seven fitted parameters were reasonable.

Results

Figure 3 displays the fitted values of K_2 at 2 and 10 Torr. Note that the 2 Torr results have been displaced vertically one unit for clarity. The two weighted least-squares lines have the same slope which shows that the rate constant k_{2a} is not pressure-dependent. Also, the values of K_2 from 303 nm experiments (open symbols in Figure 3) agree well with those from 266 nm experiments (filled symbols). The 4 Torr data show similar agreement between experiments at 266 and 303 nm, although the error bars on the 303 nm experiments are considerably larger than those at 10 Torr. At 2 Torr it was necessary to use O_2 as the carrier gas in order to keep $K_1 > K_2$ with the result that the resonance radiation was seriously attenuated during its 5 cm travel from lamp to PMT. Consequently the 303 nm experiments at 2 Torr had poor signal-to-noise ratios and so are not included in Figure 3 or in the linear least-squares fit.

TABLE 1: Values of the Rate Constants Determined from Slopes and Intercepts in Figures 3 and 4[a,b]

	2 Torr	4 Torr	10 Torr
$k_{1a}/10^{-13}$	0.953 ± 0.024	1.83 ± 0.02	3.61 ± 0.04
$k_{1b}/10^{-13}$	3.6 ± 0.3	8.3 ± 0.3	16.2 ± 0.2
k_{1c}	273 ± 35	[136]	[55]
$k_{2a}/10^{-11}$	1.736 ± 0.026	1.785 ± 0.014	1.712 ± 0.010
k_{2b}	190 ± 30	[95]	[38]

[a] Units for the rate constants are cm^3 $molecule^{-1}$ s^{-1}, except for k_{1c} and k_{2b}, which have units of s^{-1}. [b] Error limits are one standard deviation based on the scatter of data only. Values in square brackets are scaled from lower pressure values, as explained in the text.

The least-squares intercept for the 2 Torr line in Figure 3 is 190 ± 30 s^{-1}, where the ± value represents one sample standard deviation based only on the data scatter. According to the model, this should be the value of k_{2b} at 2 Torr. Similar weighted least-squares treatments for k_{2b} gave −7 ± 144 s^{-1} at 4 Torr and −40 ± 90 s^{-1} at 10 Torr. Since a zero or negative diffusion rate is unreasonable, the 2 Torr value for k_{2b} was used to estimate values for k_{2b} at higher pressures using an inverse pressure dependence. Thus the least-squares linear fits for 4 and 10 Torr were redone with fixed intercepts of 95 and 38 s^{-1}, respectively, and the results are collected in Table 1. Doing a weighted average of k_{2a} for the three different pressures and factoring in the estimated uncertainties in flow rates (8%), pressures (0.5%), and NO mixture calibration (5%), the resulting value for k_{2a} and its estimated probable error is (1.74 ± 0.16) × 10^{-11} cm^3 $molecule^{-1}$ s^{-1} at 23 °C.

Experiments to measure K_1 showed a clear pressure dependence, as expected. Since K_1 is a function of both the O_2 and NO concentrations, the fits to K_1 were made using both [O_2] and [NO] as independent variables. Most of the variation of K_1 is due to the changing oxygen concentration, but the variation in [NO] also contributes. The intercepts of the least-squares fits should give values for k_{1c}, the diffusional loss of the $CHBr_2$ radicals. While the 2 Torr fit gave a reasonable value for k_{1c} (Table 1), the 4 and 10 Torr fits gave small or negative values, 70 ± 50 and −80 ± 150 s^{-1}. As before, these were replaced with values derived from the 2 Torr fit, as was done for k_{2b}, and the least-squares fits for 4 and 10 Torr were redone using the fixed values for k_{1c} shown in Table 1.

The data and least-squares fits can be shown in two dimensions by plotting ($K_1 - k_{1b}$[NO]) vs [O_2], Figure 4a, and ($K_1 - k_{1a}$[O_2]) vs [NO], Figure 4b. The slopes of the lines in Figure 4a give values for k_{1a}, and the slopes in Figure 4b give values for k_{1b}; both are collected in Table 1. The intercepts, which are the same in Figure 4a,b, are the values for k_{1c}. The slopes increase with pressure, as expected for reactions 1a,b, both of which are three-body processes.

With values for the rate constants in hand, it is now possible to test the assumption used in the model that every dibromomethoxy radical decomposes to give a second Br atom plus CHBrO. The Yield is defined as

$$\text{Yield} = S_1/(S_0F_1F_2) \qquad \text{(III)}$$

where F_1 and F_2 are calculated using the rate constants and concentrations appropriate for each run. If every dibromomethoxy radical decomposes to give a Br, as assumed in the model, then S_1 will equal $S_0F_1F_2$ and the Yield will be unity.

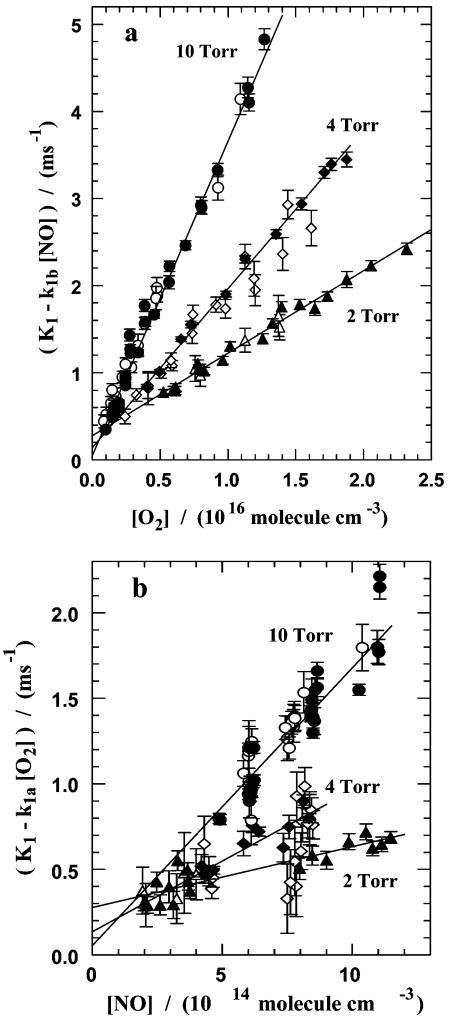

Figure 4. Dependence of K_1 on the O_2 concentration (a) and the NO concentration (b) at 2 (triangles), 4 (diamonds), and 10 Torr (circles). The open symbols are for 303 nm, and the filled symbols are for 266 nm. The solid lines are weighted linear least-squares fits. The error bars are one sample standard deviation.

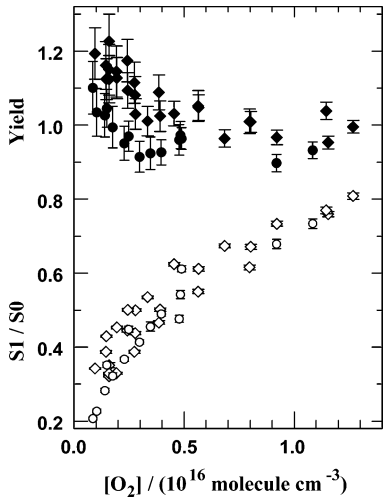

Figure 5. Ratio of amplitudes, S_1/S_0 (open symbols), and the yields (filled symbols) calculated from the amplitudes for measurements of K_1 at 10 Torr. The circles represent 303 nm runs, and the diamonds are 266 nm runs. Only the larger values of S_1/S_0 were used to calculate the average yields reported in Table 2, as discussed in the text.

TABLE 2: Weighted Average Values of Yields for Various Conditions[a,b]

λ/nm	measure	P/Torr	⟨yield⟩	s_m	N
266	K_1	10	0.993	0.0075	11
266	K_1	4	1.028	0.0051	10
266	K_1	2	0.959	0.0076	9
266	K_2	10	0.969	0.0052	15
266	K_2	4	0.989	0.0125	10
266	K_2	2	1.032	0.0054	15
303	K_1	10	0.932	0.0124	5
303	K_1	4	0.928	0.0101	9
303	K_1	2	0.901	0.0229	3
303	K_2	10	0.912	0.0104	12
303	K_2	4	0.863	0.0277	10

[a] For measurements of K_1, only the values of yield at the higher $[O_2]$ are included in the averages, as explained in the text. [b] The weighting factors were calculated by propagation of errors based on the standard deviations of S_0, S_1, the appropriate rate constants and estimated uncertainties in concentrations for each run. s_m is the sample standard deviation of the mean calculated from the N values of yield.

However, if some of the methoxy radicals react by a different route, or if the model is an inadequate description of the actual chemistry, then the calculated Yield may differ from unity.

For experiments measuring K_1, the oxygen concentrations were low and consequently values of S_1/S_0 were significantly less than 1 due to NO successfully competing with O_2 for the $CHBr_2$ radical. Figure 5 shows both the ratios of S_1/S_0 and the calculated Yields for the K_1 runs at 10 Torr. At low $[O_2]$ the values of S_1 are less than half as large as S_0; however, after correcting for the inefficiencies in stage 1 and stage 2 according to eq III, the calculated Yields are close to unity. Note that if O_2 were reacting with the $CHBr_2O$ radical before it could decompose, the Yields would drift to values less than unity at the highest oxygen concentrations; this does not occur at 2, 4, or 10 Torr, so the critical assumption that reaction 2c is fast appears to be correct.

The error bars shown in Figure 5 are derived from a propagation of error analysis. For S_1/S_0 this involves only the standard deviations of S_1 and S_0, as reported by the least-squares fitting program. Estimated errors for the Yields also include the uncertainties in rate constants and concentrations, which in turn involve estimated errors in flows and pressures for each run, and the 5% uncertainty in the NO mixture composition. As the $[O_2]$ decreases, the error bars on the Yields increase because of the larger percentage error in F_1. F_2 for the runs in Figure 5 are all close to 0.99 and therefore involve little uncertainty.

Because of the increasing errors at low $[O_2]$, only the Yields derived from values of $F_1 \geq 0.5$ were used to calculate weighted average Yields for the 10 Torr runs; these have been entered in Table 2 along with the 95% confidence limits calculated from the sample standard deviation of the mean and the Student's t distribution. Similar treatments were done for the 4 ($F_1 \geq 0.6$) and 2 Torr ($F_1 \geq 0.7$) runs.

Experiments measuring K_2 used much larger oxygen concentrations, so the amplitudes of S_1 were never very far below S_0. The products of F_1 and F_2 were always above 0.8. Consequently, all of the Yield values calculated from K_2 experiments were included in the weighted averages reported in Table 2. The weighting factors were again derived by the method of propagation of errors.

Other Bromomethanes

A quick survey was done on four other bromomethanes to see if their behavior was similar to that of bromoform. For CH_2Br_2 the absorption cross-section at 266 nm is 20 times smaller than that of bromoform,[13] but it was still possible to get some signal for bromine atoms following the laser pulse.

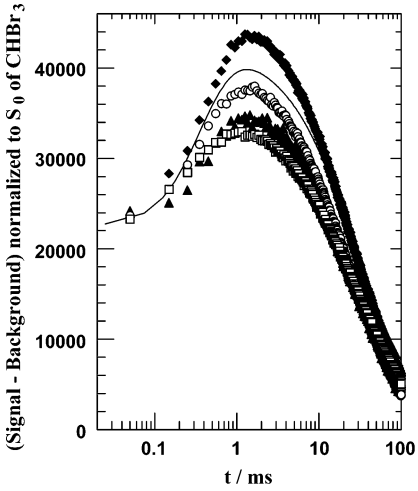

Figure 6. Bromine atom RF signals observed following photolysis of four brominated methanes at 266 nm and 10 Torr. The partial pressures of O_2 were 1.0 Torr and of NO 3.5−5 mTorr. The balance was nitrogen which had been bubbled through the liquid bromonated methanes or over solid CBr_4 at 730 Torr and 20 °C before being metered into the flow system. From the top the points represent photolysis of CBr_4 (solid diamonds), $CHClBr_2$ (open circles), CH_2Br_2 (solid triangles), and CF_2Br_2 (open squares). The solid line is a fitted trace for bromoform under similar conditions.

The CBr_4, $CHClBr_2$, and CF_2Br_2 all gave good Br signals. Since the signals had different amplitudes, because of the different cross-sections and the various pulse energies used, and different backgrounds (different attenuation of the Br resonance radiation), the signals were normalized. First the background count for each data set was subtracted from all of the bins. Then the resulting counts were scaled so that the values of S_0 were the same as that observed for bromoform for the same flow and concentrations. The resulting traces are shown in Figure 6 together with a solid line representing the fitted result for a bromoform run having comparable concentrations. All of these bromomethanes show similar behavior in that both primary and secondary bromine atoms are formed.

Discussion

The three rate constants measured in this study have not been measured previously. However, their absolute values appear reasonable when compared to those for similar reactions. For example, the rate constant measured for $CHBr_2O_2$ + NO, 1.74×10^{-11} cm^3 molecule^{-1} s^{-1}, is comparable to the rate constants for CH_2BrO_2 + NO (1.1×10^{-11}),[14] CCl_2FO_2 + NO (1.5×10^{-11}),[15] and CCl_3O_2 + NO (1.8×10^{-11}).[16]

Although k_{1a} has been determined at only three pressures, the values are less than linear in pressure indicating falloff behavior. It is possible to fit these three values to the Troe formalism[17] using a value of 0.6 for the center broadening factor. The least-squares fitted parameters are $k_\infty = 2.5 \times 10^{-12}$ cm^3 molecule^{-1} s^{-1} for the high-pressure limit and $k_o = 2.0 \times 10^{-30}$ cm^6 molecule^{-2} s^{-1} for the low. Since the measured values are much closer to the low-pressure limit than to the high, the fitted value for k_∞ is a rough estimate at best. However, this k_∞ is similar to those observed for the three chlorinated methyl radicals plus O_2 ($(2.4-2.9) \times 10^{-12}$).[18−20] The fitted value for k_o should be closer to the correct value; again it is similar to rate constants for chlorine-substituted methyl radicals reacting with O_2 ($(0.7-5) \times 10^{-30}$).[16,18−20] It should be emphasized that the above values for k_o and k_∞ are only first estimates; more reliable values must await measurements over a much broader pressure range.

Yields

The average Yields collected in Table 2 make it clear that at least for the 266 nm experiments, the Yields are close to unity at all three pressures. Taking a weighted average of the six values at 266 nm in Table 2 gives $\langle \text{Yield} \rangle = 0.994 \pm 0.007$, where the error limit represents the 95% confidence level calculated from the sample standard deviation of the mean and the Student's t distribution ($t = 2.571$ for $N = 6$). The reported average Yields in Table 2 do not always overlap unity within two or three times s_m, the sample standard deviation calculated for each mean. This suggests that there are some systematic errors that are not fully reflected in the propagation of errors treatment.

The average 303 nm Yields in Table 2 do not agree with the 266 nm result. In part this reflects the weaker signal-to-noise ratio at the longer wavelength (a factor of 3−10 depending on conditions). However, with every 303 nm Yield well below unity, the weighted average is 0.919 ± 0.016, where this 95% confidence limit does not overlap unity by a significant margin.

Orlando et al. also concluded, by observing stable products, that the $CHBr_2O$ radical predominately decomposes to give CHBrO + Br, even in 700 Torr of air.[11] However, they also observed formation of small amounts of CO, only some of which could be attributed to the thermal decomposition of the product CHBrO. They suggested that as much as 5% of the $CHBr_2O$ could be decomposing according to the reaction

$$CHBr_2O \rightarrow CBrO + HBr \quad (4)$$

followed by

$$CBrO \rightarrow CO + Br \quad (5)$$

Reaction 5 is expected to be very fast, since the Br−CO bond is thought to be very weak.[21] Consequently the present experiments, which measure only Br atoms, would still record a Yield of unity. The alternative decomposition, reaction 6, is less exothermic than reaction 4 and would not give a

$$CHBr_2O \rightarrow CHO + Br_2 \quad (6)$$

secondary Br atom. In the presence of molecular oxygen the CHO would be rapidly converted to CO.

In summary, the present yield measurements at 303 nm are consistent with the findings of Orlando et al. that CHBrO + Br are the dominant but not exclusive products of the decomposition of the dibromomethoxy radical. The minor channel of the decomposition, which does not form a Br atom but eventually generates CO, is not evident at the present time.

Interpretation of the Yields measured at 266 nm are complicated by the fact that the initial quantum yield for formation of $CHBr_2$ + Br is only 76%.[7] The other 24% of the photolysis events probably form a methylene, either CHBr + Br_2, as favored by beam experiments,[8] or CBr_2 + HBr. Either methylene is expected to react readily with O_2, although the products of these reactions are not known. Using calculated heats of formation,[22] the possible overall reactions

$$CHBr + O_2 \rightarrow CO_2 + H + Br \quad (7a)$$

$$CHBr + O_2 \rightarrow CO + OH + Br \quad (7b)$$

$$CBr_2 + O_2 \rightarrow CO_2 + Br + Br \quad (8a)$$

$$CBr_2 + O_2 \rightarrow CO + BrO + Br \quad (8b)$$

are strongly exothermic. While these possible reactions would

probably involve several steps, this does show that the generation of Br atoms from the bromonated methylenes is energetically possible.

Whatever the secondary channel is in the photolysis of bromoform at 266 nm, it seems unlikely that an alternate generation of Br atoms, such as reactions 7 or 8, would be just sufficient to bring the overall Yield values from 0.92 to essentially unity (0.994 ± 0.007). An alternative interpretation is that the superior signal-to-noise ratio available in the 266 nm experiments compared to 303 nm results in a more accurate determination of the Yield, which is really unity.

This second interpretation is supported by ab initio calculations on the three bromine-substituted methoxy radicals.[23,24] These calculations predict that all three brominated methoxy radicals are unstable with respect to dissociation along the carbon−bromine bond. The dissociations are exothermic, for $CHBr_2O$ by 20 kcal mol^{-1}, and there are no barriers to dissociation. Consequently the release of the Br atom from $CHBr_2O$ should occur within a few vibrations. In addition, the newly formed $CHBr_2O$ should retain some fraction of the 10 kcal mol^{-1} exothermicity of the reaction forming it (reaction 2a), which will ensure dissociation even if there is a small energy barrier. These predictions are supported by the studies of stable products for CH_2BrO and $CHBr_2O$, which concluded that their lifetimes were shorter than a microsecond.[11,25]

All studies to date agree that the dominant fate of the $CHBr_2O$ methoxy radical is dissociation to CHBrO + Br. Whether the yield for this reaction is just ≥90% or is really 100% cannot be decided on the basis of the experimental evidence to date.

The photolysis of the other bromomethanes shown in Figure 6 makes it clear that they all mimic bromoform. Following the initial photolytic cleavage of a carbon−bromine bond, the substituted methyl radicals react with O_2 to form peroxy radicals, which in turn react with NO to give substituted methoxy radicals. The rapid decomposition of the methoxy radicals then generates the secondary Br atom signals seen in Figure 6.

The rise times of the secondary Br signals in Figure 6 are similar, but the amplitudes of the secondary signals are different. Applying the rate constants for bromoform and the concentrations used in Figure 6, the K_1 is about 12 ms^{-1}, while K_2 is in the range of 3.5−5 ms^{-1}; i.e., reaction of the peroxy radicals with NO is probably controlling these rise times. The similar rise times observed suggest that the rate constants for the various peroxy radicals reacting with NO are not very different.

However, the ratios of S_1/S_0 in Figure 5 are different. The approximate ratios are 0.95 (CBr_4), 0.83 ($CHBr_3$), 0.73 ($CHClBr_2$), 0.57 (CH_2Br_2), and 0.50 (CF_2Br_2). These varying S_1/S_0 ratios probably reflect the varying competition between O_2 and NO for the several methyl radicals. Without knowing the rate constants involved, it is not possible to convert the measured S_1/S_0 into Yields.

The evidence in this study and in previous work suggests the generalization that any methoxy radical that contains at least one bromine atom will dissociate rapidly, even at atmospheric pressure.

Acknowledgment. We thank D. W. Toohey for loaning us the bromine lamp power supply and D. Natzic for technical assistance. The research described in this article was performed at the Jet Propulsion Laboratory, California Institute of Technology, under a contract with the National Aeronautics and Space Administration.

References and Notes

(1) Carpenter, L. J.; Liss, P. J. *J. Geophys. Res*. **2000**, *105* (20), 539.
(2) Sturges, W. T.; Oram, D. E.; Carpenter. L. J.; Penkett, S. A. *Geophys. Res. Let*. **2000**, *27*, 2081.
(3) Quack, B.; Wallace, D. W. R. *Global Biogeochem. Cycles* **2003**, *17*, 1023.
(4) Kurylo, M. J.; et al. *Scientific Assessment of Ozone Depletion: 1998*; Ennis, C. A., Ed.; World Meteorol. Organ.: Geneva, Switzerland, 1999; Chapter 2, pp 2.21−2.36.
(5) Nielsen, J. E.; Douglass, A. R. *J. Geophys. Res*. **2001**, *106*, 8089.
(6) Dvortsov, V. L.; et al. *Geophys. Res. Lett*. **1999**, *26*, 1699.
(7)) Bayes, K. D.; Toohey, D. W.; Friedl, R. R.; Sander, S. P. *J. Geophys. Res*. **2003**, *108*, 4095.
(8) Xu, D.; Francisco, J. S.; Huang, J.; Jackson, W. M. *J. Chem. Phys*. **2002**, *117*, 2578.
(9) Moortgat, G. K.; Meller, R.; Schneider, W. *The Tropospheric Chemistry of Ozone in the Polar Regions*; Niki, H., Becker, K. H., Eds.; Springer-Verlag: New York, 1993; pp 359.
(10) Vandaele, A. C.; Hermans, C.; Fally, S.; Carleer, M.; Merienne, M.-R.; Jenouvrier, A.; Coquart, B.; Colin, R. *J. Quant. Spectrosc. Radiat. Transfer* **2003**, *76*, 373. Also data file NO2R_96.DAT from Belgian Institute for Space Aeronomy.
(11) Orlando, J. J.; Tyndall, G. S.; Wallington, T. J.; Dill, M. *Int. J. Chem. Kinet*. **1996**, *28*, 433.
(12) Davies, J. W.; Green, N. J. B.; Pilling, M. J. *J. Chem. Soc., Faraday Trans*. **1991**, *87*, 2317.
(13) Molina, L. T.; Molina, M. J.; Rowland, F. S. *J. Phys. Chem*. **1982**, *86*, 2672.
(14) Sehested, J.; Nielsen, O. J.; Wallington, T. J. *Chem. Phys. Lett*. **1993**, *213*, 457.
(15) Dognon, A. M.; Caralp, F.; Lesclaux, R. *J. Chim. Phys*. **1985**, *82*, 349.
(16) Ryan, K. R.; Plumb, I. C. *Int. J. Chem. Kinet*. **1984**, *16*, 591.
(17) Troe, J. *Chem. Rev*. **2003**, *103*, 4565.
(18) Fenter, F. F.; Lightfoot, P. D.; Caralp, F.; Lesclaux, R.; Niranen, J. T.; Gutman, D. *J. Phys. Chem*. **1993**, *97*, 4695.
(19) Fenter, F. F.; Lightfoot, P. D.; Niranen, J. T.; Gutman, D. *J. Phys. Chem*. **1993**, *97*, 5313.
(20) Nottingham, W. C.; Rudolph, R. N.; Andrews, K. P.; Moore, J. G.; Tossell, J. A. *Int. J. Chem. Kinet*. **1994**, *26*, 749.
(21) Dixon, D. A.; Peterson, K. A.; Francisco, J. S. *J. Phys. Chem. A* **2000**, *104*, 6227.
(22) Dixon, D. A.; deJong, W. B.; Peterson, K. A.; Francisco, J. S. *J. Phys. Chem. A* **2002**, *106*, 4725.
(23) McGivern, W. S.; Francisco, J. S.; North, S. W. *J. Phys. Chem. A* **2002**, *106*, 6395.
(24) McGivern, W. S.; Kim, H.; Francisco, J. S.; North, S. W. *J. Phys. Chem. A* **2004**, *108*, 7247.
(25) Orlando, J. J.; Tyndall, G. S.; Wallington, J. J. *J. Phys. Chem*. **1996**, *100*, 7026.